Spin-wave velocities, density of magnetic excitations, and NMR relaxation in iron pnictides

Andrew Ong, Götz S. Uhrig,* and Oleg P. Sushkov

School of Physics, University of New South Wales, Sydney 2052, Australia

We perform an analysis of the experimentally known temperature dependence of the staggered magnetization in the antiferromagnetic phase. This analysis allows us to put an upper limit on the unknown value of the spin-wave velocity along the stripes of equal spin direction (spin stripes). The velocity is about ten times smaller than the velocity perpendicular to the spin stripes. The strongly anisotropic spin-wave dispersion implies a high density of low-energy magnetic excitations. We demonstrate that this high density strongly enhances the ^{75}As NMR spin-lattice relaxation via the Raman scattering of magnons. We derive the polarization dependence of this relaxation channel and find very good agreement with experimental data. The high density of low-energy magnetic excitations deduced from our phenomenological analysis supports the scenario that ferropnictides are close to a quantum phase transition.

PACS number(s): 74.70.−b, 75.30.Ds, 76.60.Es, 75.10.Jm

I. INTRODUCTION

One of the most important and widely discussed issues in the physics of iron pnictide superconductors is whether these materials are strongly or weakly correlated. A closely related issue is the origin of magnetism in their parent compounds. In a slightly simplistic way one can formulate the problem in the following way. Does the magnetism arise from itinerant electrons or is it due to localized electrons? For a recent review see, for instance, Ref. 1. The situation is different from cuprates where parent compounds are clearly Mott insulators and hence there is no ambiguity about the origin of magnetism.

In the present work, we do not address the issue of strong or weak correlations directly. In a phenomenological way, we analyze available experimental data on low-temperature magnetic properties and determine the previously unknown spin-wave velocity along the spin stripes, by which we refer to chains of spins running in b direction in which all the spins point in the same direction (cf. Fig. 1). This spin-wave velocity turns out to be very small. It is by an order of magnitude smaller than the velocity perpendicular to the spin stripes. The knowledge of the velocity is very important itself because it predicts the outcome of future inelastic neutron-scattering measurements. In addition, the knowledge sheds light on the issue of strong or weak correlations. The low velocity implies a high density of magnetic excitations and the high density strongly supports the strong-correlation scenario based on the vicinity to a quantum critical point.[2–5] Due to the high spectral density, magnons must contribute significantly to the NMR relaxation rate at a temperature above the spin-wave gap. We consider this mechanism for ^{75}As NMR spin-lattice relaxation and find a very good agreement between theoretical results and experimental data.

The magnetic long-range order is firmly established in the parent compounds LaFeAsO and Sr(Ba,Ca)Fe$_2$As$_2$ by neutron scattering,[6–9] muon spin resonance, and Moessbauer spectroscopy.[10,11] The neutron scattering reveals a columnar antiferromagnetic ordering with a staggered magnetic moment of $(0.3-0.4)\mu_B$ in LaFeAsO and $(0.8-0.9)\mu_B$ in Sr(Ba,Ca)Fe$_2$As$_2$. All the compounds are layered systems

consisting of Fe-As planes. For simplicity, we consider only the tetragonal lattice which is formed by the Fe ions ignoring a small orthorhombic and even monoclinic structural distortion. In Fig. 1 we show schematically the Fe-As plane and the spin ordering at the Fe sites. Along the a axis, the spin directions alternate whereas they are the same along the b axis. Spins also alternate along the c axis which is orthogonal to the plane. In our study, the lattice spacings, i.e., the distances between Fe ions, are $g_a \approx g_b \approx 2.79$ Å and $g_c \approx 6.15$ Å. We choose units such that all lattice spacings equal unity, i.e., $g_a \rightarrow 1$, $g_b \rightarrow 1$, and $g_c \rightarrow 1$. Note that the arsenic ions are shifted out of plane by $\delta c \approx \pm 1.35$ Å in a checkerboard pattern shown in Fig. 1.

The spin-wave velocities along the a and the c axis as well as the spin-wave gap at zero temperature have been measured by neutron scattering for SrFe$_2$As$_2$ (Ref. 7) and for BaFe$_2$As$_2$ (Ref. 8) as

$$v_a \approx 205 \ \text{meV},$$

$$v_c \approx 45 \ \text{meV},$$

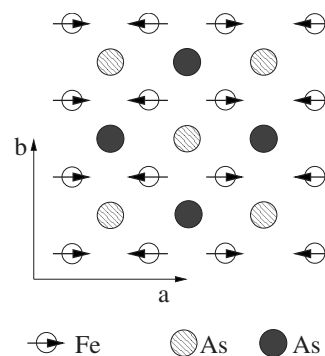$$\Delta(T=0) \approx 6.5 \ \text{meV}. \tag{1}$$

FIG. 1. The Fe-As plane. Fe ions are shown by open circles and As ions are shown by filled circles. The Fe spins are shown by arrows. The Fe ions lie exactly in the plane while As ions are out of plane by $\delta_c \approx \pm 1.35$ Å in a checkerboard pattern. The pattern is shown by different fillings of the symbols for the As ions.
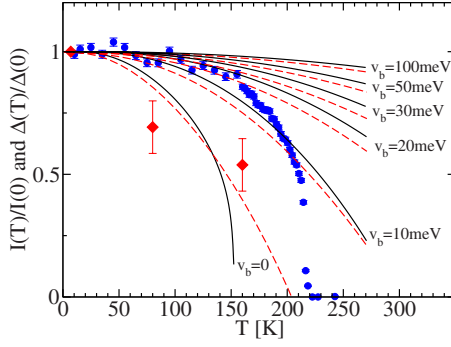
FIG. 2. (Color online) Temperature dependence of the intensity of elastic neutron scattering at the antiferromagnetic superlattice reflection and of the spin-wave gap in $SrFe_2As_2$. Points with error bars show experimental data from Ref. 7. Blue circles show the normalized neutron-scattering intensity, $I(T)/I(0)$, and red diamonds show the normalized spin-wave gap, $\Delta(T)/\Delta(0)$. The curves show theoretical results for the normalized neutron-scattering intensity for various values of the spin-wave velocity v_b along the spin stripes. Solid black curves correspond to the first scenario for the spin-wave gap, Eq. (25), and dashed red curves correspond to the second scenario, Eq. (26). The theory is justified only where the deviation of $I(T)/I(0)$ from unity is small.

But the spin-wave velocity along the b axis, i.e., along the spin stripes, has not yet been measured to our knowledge. Note that the unit-cell lattice spacings for the 122 compounds $SrFe_2As_2$ and $BaFe_2As_2$ are two times larger than the corresponding values of g, $a = 2g_a$, $b = 2g_b$, and $c = 2g_c$. The standard crystallographic convention is to set $a \to 1$, $b \to 1$, and $c \to 1$. Thus the values of the spin-wave velocities in these standard units are twice larger than the values in our units.

The Néel temperature for these compounds is $T_N = 200-220$ K. The temperature dependence of the normalized intensity of elastic neutron scattering, $I(T)/I(0)$, and the temperature dependence of the normalized spin-wave gap, $\Delta(T)/\Delta(0)$, have been measured in Ref. 7. These experimental results are shown in Fig. 2.

We are not aware of a direct measurement of the spin magnetic susceptibility of $SrFe_2As_2$. However, the data for LaFeAsO (Refs. 12 and 13) and $BaFe_2As_2$ (Ref. 14) show that the spin susceptibility in the AF ordered phase averaged over directions is about

$$\chi_s \approx 1 \times 10^{-4} \ \text{emu/(mol Fe)}. \quad (2)$$

We will use this value for $SrFe_2As_2$ keeping in mind that it might be off by a factor $\approx 1.5-2$.

II. EFFECTIVE ACTION FOR MAGNETIC EXCITATIONS

To describe spin waves we use an effective model, the nonlinear σ model with the following Lagrangian

$$L = \frac{\chi_\perp}{2}\{\dot{\vec{n}}^2 - v_a^2(\partial_a\vec{n})^2 - v_b^2(\partial_b\vec{n})^2 - v_c^2(\partial_c\vec{n})^2 + \Delta_b^2 n_a^2\}$$

$$= \frac{\chi_\perp}{2}\{(\partial_\mu\vec{n})^2 + \Delta_b^2 n_a^2\}, \quad (3)$$

where

$$\partial_\mu = (\partial_t, iv_a\partial_a, iv_b\partial_b, iv_c\partial_c), \quad (4)$$

and Δ_b is the bare spin-wave gap. The standard constraint $\vec{n}^2 = 1$ is imposed. Hereafter we set $k_B = \hbar = 1$ for simplicity. Note that generally the bare spin-wave gap Δ_b can depend on temperature if the temperature dependence arises from physics different from spin waves, say from phonons. We stress that this phenomenological description of low-energy magnetic excitations is valid independent of the specific mechanism for magnetism. The description is equally valid for magnetism caused by itinerant electrons and for magnetism caused by localized electrons. We will use Eq. (3) below the Néel temperature T_N. The field theory, Eq. (3), is the only possible effective theory that describes spin waves with dispersion $\omega_q = \sqrt{v_a^2 q_a^2 + v_b^2 q_b^2 + v_c^2 q_c^2 + \Delta^2}$. Therefore, the only important issue for the justification of Eq. (3) is that there are well-defined low-energy spin waves. This is directly supported by experiment.[7,8] According to Ref. 8 the spin waves are well defined up to $\omega \approx 150$ meV. This is an important piece of information but pragmatically, for purposes of the present work, we only need the information that spin waves exists with energies $\omega \lesssim T_N \approx 20$ meV.

The spin-wave velocities v_a and v_c are known from experiment, see Eq. (1). The susceptibility $\chi_\perp$ is related to the spin magnetic susceptibility [Eq. (2)] as

$$\chi_s = \chi_\perp \frac{2}{3}(g\mu_B)^2 N_A, \quad (5)$$

where g is the gyromagnetic ratio, μ_B is the Bohr magneton, N_A is the Avogadro constant, and the factor 2/3 comes from averaging over orientations. Lacking any other information, we take the standard value of the gyromagnetic ratio, $g = 2$. Equations (5) and (2) yield

$$\chi_\perp = 1.2 \cdot 10^{-3} 1/\text{meV}. \quad (6)$$

Due to the uncertainty in the values of χ_s and g, one has to face an uncertainty in the value of $\chi_\perp$. At worst, we estimate the uncertainty in the value of $\chi_\perp$ to be a factor 1.5–2 relative to the value given in Eq. (6).

Assuming that the system is below the Néel temperature, $\vec{n} \approx (n_a, 0, 0)$, we represent the staggered magnetizaton by

$$\vec{n} = (n_a, n_b, n_c) = (\sqrt{1 - \pi^2}, \vec{\pi}), \quad (7)$$

where the field $\vec{\pi}$ is two dimensional having only b and c components. The static component of the staggered magnetization reads in the first two leading orders

$$\langle n_a \rangle \approx 1 - \frac{1}{2}\langle \vec{\pi}^2 \rangle, \quad (8)$$

where $\langle \dots \rangle$ denotes the quantum Gibbs expectation value.

Expanding Eq. (3) in powers of $\vec{\pi}$ up to quartic terms (single-loop corrections) we obtain the following Lagrangian for the π field:

$$L = \frac{\chi_\perp}{2}\{(\partial_\mu \vec{\pi})^2 + \vec{\pi}^2(\partial_\mu \vec{\pi})^2 - \Delta_b^2 \vec{\pi}^2\}. \tag{9}$$

In order to derive the temperature-dependent quadratic effective Lagrangian L_T, one has to perform a decoupling in the quartic term in Eq. (9),

$$\vec{\pi}^2(\partial_\mu \vec{\pi})^2 \rightarrow \langle \vec{\pi}^2 \rangle (\partial_\mu \vec{\pi})^2 + \vec{\pi}^2 \langle (\partial_\mu \vec{\pi})^2 \rangle$$
$$\rightarrow \langle \vec{\pi}^2 \rangle (\partial_\mu \vec{\pi})^2 + \Delta_b^2 \vec{\pi}^2 \langle \vec{\pi}^2 \rangle. \tag{10}$$

Here we have used integration by parts and the equation of motion in leading order,

$$\partial_\mu^2 \vec{\pi} + \Delta_b^2 \vec{\pi} = 0. \tag{11}$$

Hence the decoupling yields the following effective Lagrangian:

$$L_T = \frac{\chi_\perp}{2}\{[1 + \langle \vec{\pi}^2 \rangle](\partial_\mu \vec{\pi})^2 - \Delta_b^2[1 - \langle \vec{\pi}^2 \rangle]\vec{\pi}^2\}. \tag{12}$$

After rescaling the field, $\vec{\pi}_R = \sqrt{1 + \langle \vec{\pi}^2 \rangle}\,\vec{\pi}$, we find that the spin-wave gap is renormalized as

$$\Delta(T) = (1 - \langle \vec{\pi}^2 \rangle)\Delta_b. \tag{13}$$

Following Fermi's golden rule, the scattering intensity $I(T)$ is proportional to the square of the staggered magnetization $\langle n_a \rangle^2$ which is given by Eq. (8). Combining this fact with Eq. (13) yields

$$\frac{I(T)}{I_b} = \frac{\Delta(T)}{\Delta_b} = 1 - \langle \vec{\pi}^2 \rangle + \mathcal{O}(\langle \vec{\pi}^2 \rangle^2), \tag{14}$$

where I_b is a bare scattering intensity without quantum fluctuations, for further discussion see below. For deriving this equation, we assume formally that $\langle \vec{\pi}^2 \rangle \ll 1$. We will discuss this point in more detail below.

A standard calculation of the expectation value $\langle \vec{\pi}^2 \rangle$ leads to the following result:

$$\langle \vec{\pi}^2 \rangle = \frac{1}{\chi_\perp} \int \frac{d^3q}{(2\pi)^3} \frac{1}{\omega_q}(2n(\omega_q) + 1), \tag{15}$$

where

$$\omega_q = \sqrt{v_a^2 q_a^2 + v_b^2 q_b^2 + v_c^2 q_c^2 + \Delta^2(T)} \tag{16}$$

is the spin-wave dispersion and

$$n(\omega_q) = \frac{1}{e^{\omega_q/T} - 1} \tag{17}$$

is the Bose-Einstein distribution function. The unity in the factor $(2n_q + 1)$ in Eq. (15) is due to quantum fluctuations which lead to the quantum renormalization of the bare spin-wave gap, $\Delta_b(T) \rightarrow \Delta_{qr}(T)$, and to the concomitant renormalization of the bare scattering intensity, $I_b \rightarrow I_{qr}(T)$. The quantitative outcome of this renormalization depends on the high-energy cutoff

$$\frac{I_{qr}}{I_b} = \frac{\Delta_{qr}}{\Delta_b} = 1 - \frac{1}{\chi_\perp} \int \frac{d^3q}{(2\pi)^3} \frac{1}{\omega_q}. \tag{18}$$

In our study, we include the case where the quantum renormalized quantities retain a temperature dependence from a temperature-dependent $\Delta_b(T)$, whose dependence is induced from physical effects outside of the nonlinear σ model, for instance from structural changes or phonons. The quantum renormalized quantities equal the physical ones at zero temperature, $\Delta(0) = \Delta_{qr}(0)$ and $I(0) = I_{qr}(0)$. Note that I_b is temperature independent by definition.

On the present single-loop level, the temperature effects can be accounted for by

$$\frac{I(T)}{I_{qr}(T)} = \frac{\Delta(T)}{\Delta_{qr}(T)} = 1 - \langle \vec{\pi}^2 \rangle_{\text{therm}} \tag{19a}$$

$$\langle \vec{\pi}^2 \rangle_{\text{therm}} = \frac{1}{\chi_\perp} \int_0^\infty \rho(\omega, \Delta(T))n(\omega)d\omega \tag{19b}$$

instead of Eqs. (14) and (15). Here we use the density of magnetic excitations $\rho(\omega, \Delta)$ which reads in three dimensions

$$\rho(\omega, \Delta) = \frac{1}{\pi^2 v_a v_b v_c} \omega \sqrt{\omega^2 - \Delta^2}\,\Theta(\omega - \Delta). \tag{20}$$

The above continuum expressions in three dimensions are only valid if v_b is not very small compared to temperature, $v_b \pi \gg T$, because for dominating temperature, the boundaries of the Brillouin zone are felt which are not captured by the non linear σ model. In the opposite limit, $v_b \pi \ll T$, one should use the two-dimensional density of

$$\rho(\omega, \Delta) = \frac{1}{\pi v_a v_c} \omega \Theta(\omega - \Delta). \tag{21}$$

We point out that for temperature-independent bare gap Δ_b, we have $I_{qr}(T) = I(0)$ and $\Delta_{qr}(T) = \Delta(0)$. Then Eq. (19a) already provides the result to be compared with experiment. Both normalized quantities, gap and intensity, should display the same temperature dependence in their deviation from unity. For this reason they are depicted in the same plot in Fig. 2. We will discuss the very different behavior of both experimental quantities below.

Equation (19a) does not yet provide the ratio $I(T)/I(0)$ given by experiment if Δ_b is temperature dependent. To obtain full knowledge about $I(T)/I(0)$, we have to account for the influence of the infrared cutoff, i.e., the gap, on the quantum renormalization. We find

$$R_{qr}(T) := \frac{I_{qr}(T)}{I_{qr}(0)} \tag{22a}$$

$$= 1 - \frac{1}{2\chi_\perp} \int_0^\Lambda d\omega \frac{\rho(\omega, \Delta_{qr}(T)) - \rho(\omega, \Delta_{qr}(0))}{\omega}, \tag{22b}$$

where we introduce a high-energy (UV) cutoff Λ to ensure convergence. A realistic estimate is $\Lambda = 200$ meV.[5,8] Note that the difference occurring in Eq. (21) depends only

weakly, i.e., logarithmically on the precise value of Λ. In two dimensions, there is even no dependence at all on the UV cutoff.

The final result is obtained by combining Eqs. (19a) and (21) in

$$\frac{I(T)}{I(0)} = \frac{I(T)}{I_{qr}(T)} \cdot \frac{I_{qr}(T)}{I_{qr}(0)} = [1 - \langle \vec{\pi}^2 \rangle_{\text{therm}}] R_{qr}(T), \quad (23)$$

where $I_{qr}(0) = I(0)$ entered.

A remark on the validity of the single-loop approximation is in order. Obviously, the theoretical expressions are only valid if the thermal renormalization remains small, i.e., $\delta I / I(0) \ll 1$ and $\delta I = I(0) - I(T)$. Therefore, one cannot rely on Eq. (23) in the vicinity of the critical point. But we can rely on Eq. (23) at $T < 200$ K where, according to experimental data, $\delta I / I(0) < 0.3$.

III. VALUE OF THE GYROMAGNETIC RATIO AND POSSIBLE ORBITAL DYNAMICS

In the present work we use the standard value $g = 2$ which is the spin gyromagnetic ratio. This scenario assumes that the magnetism in the system is entirely due to spins but the orbital physics of iron is certainly more complex and spin-orbit coupling plays an important role.[15] So values of the g factor or g tensor different from a scalar value of 2 are quite possible.

The phenomenological nonlinear σ-model description is valid independent of the origin of magnetism. Therefore, our conclusions in the present paper do not depend on the extent that orbital and/or charge degrees of freedom play a major role. Only the precise numerical estimates depend on the numerical value of g. So for the present paper a better knowledge of g will affect only the numerical estimates and not the scenario. But for microscopic considerations, for instance, the issue which value of spin is most appropriate, the local-orbital physics is of fundamental importance and measurements of g can shed light on this issue.

We are not aware of data on the value of g. Hence we would like to point out that the large value of the spin-wave gap, $\Delta(0) = 6.5$ meV, gives a unique opportunity to measure g by inelastic neutron scattering. If a magnetic field $\mathcal{B}$ is applied, that is, directed along the a axis, the spin-wave excitations will be shifted in energy according to their projection of the angular momentum by ± 1 along a. Therefore, the magnetic field will split the spin-wave gap in two,

$$\Delta_- = 6.5 \text{ meV} - g\mu_B \mathcal{B}, \quad (24a)$$

$$\Delta_+ = 6.5 \text{ meV} + g\mu_B \mathcal{B}. \quad (24b)$$

For $\mathcal{B} = 15$ T and for $g = 2$, the splitting takes the value $2g\mu_B \mathcal{B} \approx 3.5$ meV so that it should be easily observable in neutron spectra.

IV. ANALYSIS OF EXPERIMENTAL DATA

For explicit calculations we need to specify the temperature dependence of the quantum renormalized gap Δ_{qr}. Since

we do not have experimental knowledge about this quantity, we study two scenarios which correspond to opposite limits. It will turn out that our conclusions depend only weakly on which scenario is realized.

The spin-wave gap is caused by spin-orbit interaction in combination with the orthorhombic lattice deformation. The deformation is practically temperature independent below T_N. Hence the scenario (i) assumes that the quantum renormalized spin-wave gap Δ_{qr} is temperature independent. Then the observed spin gap acquires its temperature dependence $\Delta(T)$ solely from Eq. (19a). The zero-temperature value is fixed to

$$\Delta_{qr} = \Delta(0) = 6.5 \text{ meV}, \quad (25)$$

and the temperature dependence of the physical gap $\Delta(T)$ is determined by the self-consistent solution of Eqs. (1), (6), (19a), (19b), (20), and (21). However, according to Eq. (19a), this scenario implies the identical temperature dependence of the normalized neutron intensity and of the normalized spin-wave gap. This consequence is not supported by experiment. According to the data from Ref. 7 shown in Fig. 2, the dependencies are significantly different. But it cannot be excluded that experimental difficulties, for instance the influence of the charge degrees of freedom, prevent the reliable measurement of the spin gap at finite temperature. So it is instructive to consider scenario (i) as one limiting case.

In scenario (ii), we assume that the quantum renormalized gap Δ_{qr} is temperature dependent in precisely such a way that the experimentally observed $\Delta(T)$ shown in Fig. 2 is induced. The temperature dependence $\Delta_{bR}(T)$ may result from the influence of low-energy phonons. In this case, we fit the experimental data[7] for $\Delta(T)$ by the linear function

$$\Delta(T) = 6.5 \text{ meV} - 0.020T \text{ meV/K}. \quad (26)$$

Then we employ Eqs. (1), (6), (19a), (19b), (20), and (21) to calculate the neutron-scattering intensity resulting from the phenomenological spin-wave gap, Eq. (26).

The theoretical results obtained in the two scenarios for the values of the spin-wave velocity along the spin stripes $v_b = 100$, 50, 30, 20, 10, and 0 meV are displayed in Fig. 2. The solid black curves correspond to scenario (i), i.e., Eq. (25). The dashed red curves correspond to scenario (ii), i.e., Eq. (26).

We emphasize that both scenarios for the temperature dependence of the spin-wave gap yield almost coinciding curves for the neutron-scattering intensity. This can be attributed to the fact that by construction both scenarios are equal at $T = 0$ so that the difference between them can only be discerned at sufficiently large temperature. But if $T \gtrsim \Delta(T)$, the precise value of the spin-wave gap does not matter anymore.

We already pointed out that the comparison between theoretical and experimental data makes sense only below 180–200 K where $\delta I / I(0)$ is sufficiently small and the theory is quantitatively reliable. The curves with $v_b = 100$ meV and $v_b = 50$ meV clearly disagree with experiment, while the curves with $v_b = 30$ meV and $v_b = 10$ meV constitute upper and lower bounds to the experimental data. The curve for $v_b = 20$ meV is in good agreement with the data in the range
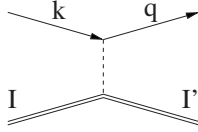
FIG. 3. Magnon Raman scattering on nuclear spin due to hyperfine interaction. Solid lines denote magnons, the double lines denote a nuclear spin. The dashed line denotes the hyperfine interaction.

of its validity ($\delta I/I \ll 1$). The three-dimensional (3D) formula (20) is at the verge of its validity for $v_b = 10$ meV since $v_b \pi \approx T$. Therefore, in Fig. 2, we also include curves for $v_b = 0$ which are obtained using the two-dimensional (2D) formula (21). We also studied the 3D→2D crossover empirically replacing $v_b^2 q_b^2$ by $4v_b^2 \sin^2(q_b/2)$ in Eq. (16). We do not show the corresponding curves because they completely confirm the results shown in Fig. 2.

Thus, our conclusion is that the value of the spin-wave velocity along spin stripes, v_b, is in the range

$$v_b \approx 10 - 30 \text{ meV}, \quad (27)$$

which means it is at least ten times smaller than $v_a \approx 205$ meV. We stress that in essence this conclusion is based on the density of magnetic excitations [Eq. (20)]. The number of excitations at low energies govern the thermally induced reduction in the staggered magnetic moment. If v_b is large, the density is low implying a weak temperature dependence of the elastic neutron-scattering intensity. If v_b is small, the density is large implying a strong temperature dependence of the elastic neutron-scattering intensity. The value of v_b must be sufficiently low to produce the experimentally found temperature dependence of the scattering intensity.

The very low value of v_b that follows from the experimental result for $I(T)$ implies that magnetic fluctuations play a prominent role in the ferropnictides. This supports the previously proposed scenario that the ferropnictides are systems close to a quantum phase transition.[5]

V. NMR SPIN-LATTICE RELAXATION FOR ^{75}As

As an additional test bed for our scenario of strong magnetic fluctuations at low energies, we study the NMR relaxation rate T_1^{-1}. This relaxation is due to inelastic Raman-type scattering of thermally excited magnons from nuclear spin, see Fig. 3.

Clearly, this mechanism is most important at temperatures above the spin-wave gap. For concreteness, we consider the relaxation of the nuclear spin of ^{75}As. The As ion is positioned at the top of a pyramid with four Fe ions at its base, see Fig. 1. The hyperfine interaction of the ^{75}As nuclear spin I with the electronic spin S on the adjacent Fe ion is of the following form:[16]

$$H = B(\vec{I} \cdot \vec{S}) + C(\vec{I} \cdot \vec{N})(\vec{S} \cdot \vec{N}), \quad (28)$$

where $\vec{N}$ is a unit vector directed from As to Fe, see Fig. 1. The B term is due to s-wave transferred hyperfine interaction and the C term is due to p-wave transferred hyperfine inter-

action. It is known[16] that the effective static hyperfine magnetic field at As takes the value $B_{\text{eff}} \approx 1.5$ T and is directed along the c axis. The average electronic magnetic moment at the Fe site is $\approx 0.8 \mu_B$.[7,8] Assuming that $g=2$, this implies an average static spin component of $\langle S \rangle \approx 0.4$. Since the electronic spins are arranged in a staggered pattern, see Fig. 1, only the C term in Eq. (28) contributes to the effective static field. Hence

$$\mu_n B_{\text{eff}} = 4 \times 0.4 \times 0.33 \times C \times I, \quad (29)$$

where $I=3/2$ is the nuclear spin and $\mu_n = 1.86 \mu_N$ is the magnetic moment of the ^{75}As nucleus. The factor 4 in Eq. (29) stems from the four neighboring Fe ions and $0.33 = N_a N_c$ is a product of components of the unit vector $\vec{N}$ in the geometry of the As-Fe^4 pyramid. From Eq. (29) we find

$$C \approx 1.1 \times 10^{-4} \text{ meV} \rightarrow 27 \text{ MHz}. \quad (30)$$

Alternatively, the rescaling from the known values of transferred hyperfine constants in cuprates yields the following estimates

$$B \approx 10^{-3} \text{ meV} \rightarrow 250 \text{ MHz}, \quad (31a)$$

$$C \approx 10^{-4} \text{ meV} \rightarrow 25 \text{ MHz}. \quad (31b)$$

While the estimate for C agrees very well with Eq. (30) deduced from the experimental data,[16–18] the estimate in Eq. (30) for B is about five times larger than the one measured in Ref. 16. It is worthwhile noting that there is a comment in Ref. 16 that they might underestimate the value of B. In the present work, we will rely on the value of C given in Eq. (30) and on the estimate for B given in Eq. (30). It is very natural that $B \gg C$ because B is due to the s-wave and C is due to the p-wave hyperfine interaction.

The static components of the electron spins are polarized along the a axis, see Fig. 1. Hence the spin-wave excitations are polarized along the b and the c axis. To describe the magnon Raman process shown in Fig. 3, we need only the part of Eq. (28) which is bilinear in spin-wave creation and annihilation operators, i.e., bilinear in $\vec{\pi}$ in the language of the nonlinear σ model. This implies that we only need to keep the terms in Eq. (28) that are proportional to the a component of the electron spin S,

$$H \rightarrow (BI_a + 0.33 CI_c) \sum_i S_{ai}, \quad (32)$$

where the summation goes over four nearest Fe sites. Finally, in the notation of the σ model, $\vec{S}/S_{\text{eff}} \rightarrow \vec{n} = (n_a, n_b, n_c) = (\sqrt{1-\pi^2}, \vec{\pi})$, which leads to

$$H \rightarrow \delta(\mathbf{r}) S_{\text{eff}} (2BI_a \partial_a + 40.33 CI_c) n_a$$
$$\rightarrow \delta(\mathbf{r}) S_{\text{eff}} (BI_a \partial_a + 0.66 CI_c) \vec{\pi}^2, \quad (33)$$

where constant terms are omitted in passing to the last line. The gradient ∂_a along the a axis in the B term appears because the magnetization in this direction is staggered. We remind the reader that in our notations both $\delta(\mathbf{r})$ and ∂ are dimensionless. In Eq. (33) we have introduced the effective spin S_{eff}. The first naive impression is that $S_{\text{eff}} = \langle S \rangle \approx 0.4$. This would imply that the magnon Raman operator is renor-

malized by quantum fluctuations exactly like the staggered magnetization. However, we have checked by an explicit single-loop calculation that the Raman operator is not renormalized while the staggered magnetization is certainly reduced in the single-loop approximation. So the naive expectation is wrong. For numerical estimates we will use

$$S_{\text{eff}} = 1. \tag{34}$$

It is clear from the kinematic structure of Eq. (33) that the B term contributes to the spin-lattice relaxation only if the initial nuclear spin is directed perpendicular to the a axis. The C term contributes to the relaxation only if the initial nuclear spin is directed perpendicular to the c axis. The Raman relaxation rate due to the B term is given by Fermi's golden rule

$$W_B = 2\pi \frac{[S_{\text{eff}}B]^2}{V^2}$$
$$\times \sum_{\mathbf{k},\mathbf{q}} \frac{(k_a - q_a)^2}{\chi_\perp^2 \omega_k \omega_q} n_k (1 + n_q) \delta(\omega_k - \omega_q - \omega_{\text{NMR}}). \tag{35}$$

The factor $2\pi = 2 \times \frac{1}{2} \times 2\pi$ is the factor 2π from Fermi's golden rule multiplied by the number of magnon polarizations, 2, and multiplied by $\frac{1}{2}$ resulting from Clebsch-Gordon coefficients related to the nuclear spin $I = 3/2$. The factor $(\chi_\perp^2 \omega_k \omega_q)^{-1}$ is due to the normalization of the $\vec{\pi}$ field, the factor $(k_a - q_a)^2$ is due to the gradient ∂_a, and n_q is given by Eq. (17). Since the NMR frequency is very small, $\omega_{\text{NMR}} \ll \omega_q$, the expression (35) can be transformed to

$$W_B = \frac{[S_{\text{eff}}B]^2}{12\pi^3 (\chi_\perp v_a v_b v_c)^2} \frac{1}{v_a^2} \int_\Delta^\infty \frac{(\omega^2 - \Delta^2)^2}{\sinh^2(\omega/2T)} d\omega, \tag{36}$$

where Δ is the spin-wave gap. The two factors $(\omega^2 - \Delta^2)$ in the numerator of the integrand stem from the density of states in three dimensions and from the matrix element $(k_a - q_a)^2$.

Similarly, the Raman relaxation rate due to the C term reads

$$W_C = \frac{[S_{\text{eff}}0.66C]^2}{8\pi^3 (\chi_\perp v_a v_b v_c)^2} \int_\Delta^\infty \frac{(\omega^2 - \Delta^2)}{\sinh^2(\omega/2T)} d\omega, \tag{37}$$

where there is one factor $(\omega^2 - \Delta^2)$ less in the numerator because there is no particular momentum-dependent matrix element.

It is clear that Eqs. (36) and (37) are not justified in the vicinity of the Néel temperature. Obviously, they are not valid at $T > T_N$ either. So we use them only below T_N. Both W_B and W_C are very steep functions of temperature. Plots of W_B and W_C calculated with parameters given by Eqs. (1), (6), (30), and (34) and $v_b = 20$ meV are presented in Fig. 4. The decay rate W_C is much smaller than W_B, $W_B \gg W_C$, and hence $1/T_1 \approx W_B$ so that the magnon Raman relaxation is mainly due to the s-wave transferred hyperfine interaction. The estimate for the value of relaxation rate presented in Fig. 4 agrees with the available data.[16–18]
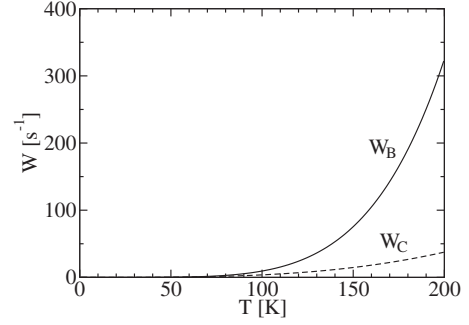

FIG. 4. NMR relaxation rates due to magnon scattering. The solid curve gives contribution of the s-wave transferred hyperfine coupling, see Eq. (36). The dashed curve gives contribution of the p-wave transferred hyperfine coupling, see Eq. (37). The parameters are given by Eqs. (1), (6), (30), and (34) and $v_b = 20$ meV.

One can fit the data by fine tuning of B and/or v_b and/or $\chi_\perp$. But this is not our aim here. Note, however, that the NMR relaxation rate, Eq. (36), is proportional to the second power of the density of magnetic excitations, Eq. (20). So it is very sensitive to the value of ρ in Eq. (20) and hence to the value of v_b. Hence the fact that our previous set of parameters yield the correct magnitude of the NMR relaxation rate strongly supports our claim that v_b is small.

Since the relaxation is dominated by W_B, we predict a significant polarization dependence of the relaxation. The corresponding Hamiltonian contains only the a component of the nuclear spin, see Eqs. (32) and (33). Therefore, this mechanism does not contribute to relaxation if the ^{75}As nuclear spin is polarized along the a axis. The mechanism contributes equally for polarizations along the b and the c axis. For a twinned sample, where domains with swapped a and b axes are of equal weight, this argument implies that the relaxation for the c polarization of nuclear spin is two times faster than the relaxation for an in-plane polarization of the nuclear spin.

For temperatures below the spin-wave gap the magnon Raman relaxation is essentially switched off. In other words, the mechanism related to collective magnetic modes is not active. But there is also a diffuse magnetic relaxation stemming from the charge degrees of freedom because the system is not an insulator. It is natural to assume that this diffuse relaxation scales linearly with temperature as it does in normal Fermi liquids. This low-temperature behavior of the relaxation was observed in Refs. 16 and 18. The charge-driven relaxation is certainly also active for $T > \Delta$, but in this regime, its contribution to the NMR relaxation rate is relatively small with the contribution from collective magnetic modes prevailing.

VI. CONCLUSIONS

We studied the parent ferropnictides below their Néel temperature. Based on the nonlinear σ model, we considered the available experimental data on the temperature dependence of the staggered magnetization phenomenologically. We found that one needs a high density of magnetic excitations to explain the relatively strong temperature dependence

of the magnetization. This implies that the spin-wave velocity along the spin stripes is very small. The values for this velocity estimated from the analysis are $v_b \approx 10-30$ meV. For comparison, the in-plane velocity perpendicular to stripes takes the value $v_a \approx 205$ meV.

We also analyzed the NMR spin-lattice relaxation rate for ^{75}As. Due to their high spectral density, the magnons dominate the relaxation rate at temperatures above the spin-wave gap. Our estimates for the relaxation rate based on the density found from the neutron-scattering data agree very well with direct NMR measurements. This is an independent confirmation of the high spectral density of magnetic excitations.

So both the temperature-dependent magnetization as well as the NMR relaxation rate confirm strong magnetic fluctuations at low energies. Thus the present phenomenological analysis corroborates the scenario that the ferropnictides constitute systems close to a quantum phase transition triggered by frustrated magnetic couplings.[5] Hence a strongly correlated picture of the ferropnictides is favored.

Very recent inelastic neutron-scattering data[19,20] indicate the ratio of spin-wave velocities $v_a/v_b \approx 2$. This is not consistent with our conclusion $v_a/v_b \approx 10$. Our analysis of the temperature dependence of the staggered magnetization and especially of the NMR relaxation rate is in essence based only on the spin-wave dispersion, Eq. (16). Only the dispersion determines the density of excited magnons at a given temperature and only the density determines the NMR relaxation rate. With the spin-wave velocity v_b taken from[19,20] one obtains the relaxation rate about 20–30 smaller than the experimental one.

How can the above discrepancy be explained? The data[19,20] is taken on twinned samples because only below the structural-transition temperature, the orthorhombicity occurs. Superposing dispersions with prominent ridges such as the ones in Fig. 3a in Ref. 5 can lead to responses similar to the ones in Refs. 19 and 20 for moderate and high energies. The time-of-flight technique used in both experimental probes[19,20] is certainly best suited for investigating the moderate and higher energies.

If the careful study of the influence of twinning does not solve the discrepancy, our analysis indicates the existence of some low-energy ($\approx 10-20$ meV) magnetic degrees of freedom which have not been taken into account so far. These degrees of freedom must contribute to the NMR relaxation and they must be difficult to detect by neutron scattering.

From our results and the above discussion, we conclude that further experiments focusing on low-lying magnetic modes are called for to resolve this crucial issue. It would be highly desirable if low-temperature detwinned samples could be generated.

*On leave from Lehrstuhl für Theoretische Physik I, Technische Universität Dortmund, Otto-Hahn Straße 4, 44221 Dortmund, Germany

[1] I. Mazin and J. Schmalian, arXiv:0901.4790 (unpublished).

[2] C. Fang, H. Yao, W. F. Tsai, J. P. Hu, and S. A. Kivelson, Phys. Rev. B **77**, 224509 (2008).

[3] C. Xu, M. Müller, and S. Sachdev, Phys. Rev. B **78**, 020501(R) (2008).

[4] D.-X. Yao and E. W. Carlson, Phys. Rev. B **78**, 052507 (2008).

[5] G. S. Uhrig, M. Holt, J. Oitmaa, O. P. Sushkov, and R. R. Singh, Phys. Rev. B **79**, 092416 (2009).

[6] C. de la Cruz, Q. Huang, J. W. Lynn, J. Li, W. Ratcliff, J. L. Zarestky, H. A. Mook, G. F. Chen, J. L. Luo, N. L. Wang, and P. Dai, Nature (London) **453**, 899 (2008).

[7] J. Zhao *et al.*, Phys. Rev. Lett. **101**, 167203 (2008).

[8] R. A. Ewings, T. G. Perring, R. I. Bewley, T. Guidi, M. J. Pitcher, D. R. Parker, S. J. Clarke, and A. T. Boothroyd, Phys. Rev. B **78**, 220501(R) (2008).

[9] R. J. McQueeney *et al.*, Phys. Rev. Lett. **101**, 227205 (2008).

[10] H.-H. Klauss *et al.*, Phys. Rev. Lett. **101**, 077005 (2008).

[11] H. Luetkens *et al.*, Nature Mater. **8**, 305 (2009).

[12] F. Ning, K. Ahilan, T. Imai, A. S. Sefat, R. Jin, M. A. McGuire, B. C. Sales, and D. Mandrus, J. Phys. Soc. Jpn. **77**, 103705 (2008).

[13] R. Klingeler, N. Leps, I. Hellmann, A. Popa, C. Hess, A. Kondrat, J. Hamann-Borrero, G. Behr, V. Kataev, and B. Büchner, arXiv:0808.0708 (unpublished).

[14] F. Ning, K. Ahilan, T. Imai, A. S. Sefat, R. Jin, M. A. McGuire, B. C. Sales, and D. Mandrus, J. Phys. Soc. Jpn. **78**, 013711 (2009).

[15] J. Wu, P. Phillips, and A. H. Castro Neto, Phys. Rev. Lett. **101**, 126401 (2008).

[16] K. Kitagawa, N. Katayama, K. Ohgushi, M. Yoshida, and M. Takigawa, J. Phys. Soc. Jpn. **77**, 114709 (2008).

[17] S.-H. Baek, N. J. Curro, T. Klimczuk, E. D. Bauer, F. Ronning, and J. D. Thompson, Phys. Rev. B **79**, 052504 (2009).

[18] N. J. Curro and A. P. Dioguardi, N. ApRoberts-Warren, A. C. Shockley, and P. Klavins, New J. Phys. **11**, 075004 (2009).

[19] S. O. Diallo, V. P. Antropov, T. G. Perring, C. Broholm, J. J. Pulikkotil, N. Ni, S. L. Bud'ko, P. C. Canfield, A. Kreyssig, A. I. Goldman, and R. J. McQueeney, Phys. Rev. Lett. **102**, 187206 (2009).

[20] J. Zhao, D. T. Adroja, D.-X. Yao, R. Bewley, S. Li, X. F. Wang, G. Wu, X. H. Chen, J. Hu, and P. Dai, Nat. Phys. (to be published).